POLARIMETRIC PHASE RATIOS OF THE LUNAR SURFACE. Y. G. Shkuratov[1], N. V. Opanasenko[1], V. G. Kaydash[1], G. Videen[2], V. V. Korokhin[1], Sungsoo S. Kim[3], Minsup Jeong[4], Young-Jun Choi[4], [1]Institute of Astronomy, V. N. Karazin National University, 35 Sumska St, Kharkiv, 61022, Ukraine, [2]Space Science Institute, 4750 Walnut St. Suite 205, Boulder CO 80301, USA, [3]Dept. of Astronomy and Space Science, Kyung Hee University, Yongin, Kyungki 17104, Korea. [4]Korea Astronomy and Space Science Institute, Daejeon 34055, Korea.

Introduction: Phase dependences of lunar apparent albedo $A(\alpha)=A_{\perp}(\alpha)+A_{\parallel}(\alpha)$ and polarization degree $P(\alpha)=[A_{\perp}(\alpha)-A_{\parallel}(\alpha)]/[A_{\perp}(\alpha)+A_{\parallel}(\alpha)]$, where $A_{\perp}(\alpha)$ and $A_{\parallel}(\alpha)$ are the polarization components perpendicular and parallel to the photometric equator, and α is the phase angle, can be roughly characterized by slopes of the phase functions $A(\alpha)$ and $P(\alpha)$ between different α_1 and α_2. The slopes of $A(\alpha)$ are dominated by the shadowing effect that increases with increasing surface roughness [1,2]. The function $P(\alpha)$ rather is related to single particle scattering [2], hence, its slopes may characterize the polarimetric scattering indicatrix of single particles. In the case of the lunar surface the incoherent multiple scattering also takes place, decreasing all $A(\alpha)$ and $P(\alpha)$ slopes.

The photometric phase-ratio method [3] has been used to study structure variations of the lunar surface. For instance, it allows investigations of spacecraft landing sites [4-6] and fresh lunar surface of young craters walls [2,7]. The investigations revealed the effect of scouring and smoothing caused by the impact of the gas jets from the rocket engines that destroy the primordial "fairy castle" structure that effectively produces the shadow effect. Polarimetry also may suggest information about the structure of the lunar surface [2,8]. It can be used, in particular, for assessing variations of the average size of regolith particles and lunar surface porosity.

If there are polarimetric images obtained at phase angles α_1 and α_2, different ratios of the polarization components, e.g., $A_{\perp}(\alpha_1)/A_{\perp}(\alpha_2)$, $A_{\parallel}(\alpha_1)/A_{\parallel}(\alpha_2)$, or $P(\alpha_1)/P(\alpha_2)$, can be calculated. We here study such ratios for the western portion of the lunar disk using telescope observations, considering $\alpha_1 > \alpha_2$.

Data and Processing: The lunar imaging campaign was organized in 2010 with the 60-cm reflector at the Maidanak Observatory (Uzbekistan) [9,10]. We used Canon EOS 550D cameras as image detectors (CMOS) for regional scanning in three wide spectral bands (λ_{eff} = 0.47, 0.52, 0.61 μm) at different phase angles. A rotated polarizing filter was exploited to register lunar images. We converted the pixel counts to numbers proportional to brightness of the lunar surface, carrying out corrections for every initial image, accounting for dark current, non-linearity, instrumental light scattering, and flat field.

The construction of polarimetric and phase ratios demands a unification of source images, e.g., compensation for the global (limb-terminator) brightness trend. For this we used Akimov's formula [2]. To derive phase-function slopes we perform coregistering of two suitable images in a pair with sub-pixel accuracy and obtain the phase-ratio image by dividing their corresponding pixels; the most reliable results can be obtained if the rubber-sheet algorithm for coregistration is used [11]. All the frames are mapped into the same cartographic projection. We here used images acquired at α_2 = 63º and α_1 = 87º and at λ_{eff} = 0.52 μm.

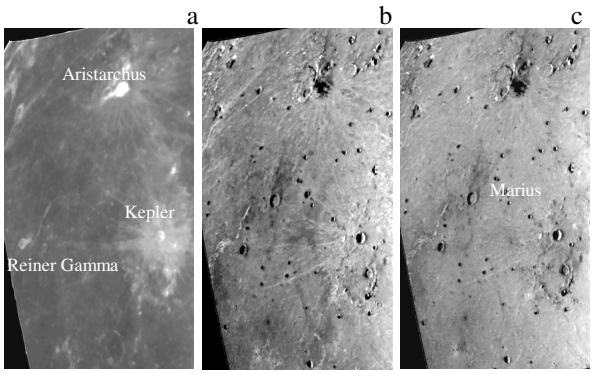

Figure 1 (a): Equigonal albedo calculated at α=63º, (b): Phase ratio $R_{\parallel}$(87º/63º), and (c): $R_{\perp}$(87º/63º)

Results and Discussion: Figure 1a shows the equigonal albedo map calculated at α = 63º. This albedo corresponds to the apparent albedo when the global brightness trend is removed [2]. The craters Aristarchus and Kepler as well as Reiner Gamma formation are marked. Maps of ratios $R_{\parallel}=A_{\parallel}(87º)/A_{\parallel}(63º)$ and $R_{\perp}=A_{\perp}(87º)/A_{\perp}(63º)$ are shown in Fig. 1b and c, respectively. As can be seen, there are differences between these ratios. For instance, the contrast of the Kepler ray system and especially Reiner Gamma formation in the perpendicular component is greatly diminished compared to the parallel component case. This also has been noted in [12]. The topography is enhanced in the phase-ratio images; for instance, the crater Marius appears in Fig. 1b and c. Moreover, the surrounding region of crater Marius reveals a structure resembling a butterfly pattern that is characteristic of oblique impacts at crater formation. This butterfly pattern is visible in both components, although it is enhanced in $R_{\perp}$.

The differences between the $R_\perp$ and $R_\parallel$ images also can be informative. Both the parallel and perpendicular components contribute all orders of scattering. However, in the cases of small and large particles, single-particle scattering produces chiefly perpendicularly polarized light at large phase angles. Thus, the images shown in Fig. 1b and c characterize variations of the difference between low- and high scattering orders, which should be correlated with albedo.

Figure 2a represents the ratio $R_\perp(87°/63°)/R_\parallel(87°/63°)$ (a ratio of ratios) that, as one can see, inversely correlates with apparent albedo $A(63°)=A_\perp(63°)+A_\parallel(63°)$. We have studied this correlation finding that it is almost linear on a log-log scale. Then we calculate the distribution of a parameter that characterizes deviations from the regression line of the correlation between log$A$ and log$(R_\perp/R_\parallel)$ (see Fig. 2b); i.e., we remove the albedo component from Fig. 2a. The map of this parameter is shown in Fig. 2b, revealing a detailed pattern that may reflect the complicated geologic history of the region under study.

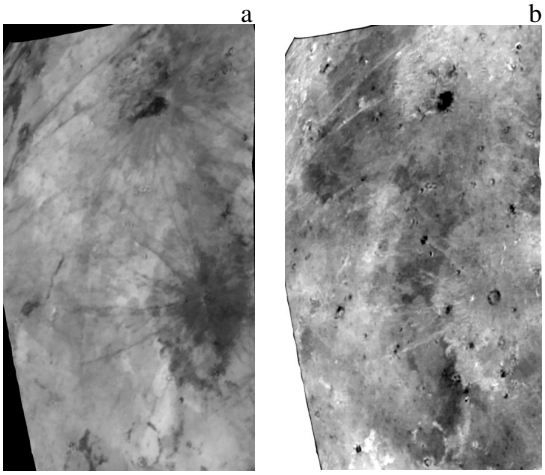

Figure 2 (a): Ratio of the images shown in Fig. 1b, i.e. $R_\perp/R_\parallel$; (b): Map of deviation from the regression line of the correlation between log$A$ and log$(R_\perp/R_\parallel)$

We also have studied the phase ratios of other polarimetric parameters. Fig. 3a shows the polarization degree distribution determined at α=63°, i.e. $P(63°)=[A_\perp(63°)–A_\parallel(63°)]/[A_\perp(63°)+A_\parallel(63°)]$. As can be anticipated, this parameter reveals a strong inverse correlation with albedo (the Umov law). Deviations from such correlations have been studied in [2,8,9,13,14]. We calculate the ratio $P(87°)/P(63°)$ shown in Fig. 3b. As in the case of Fig. 2a, this closely correlates with the inverse albedo pattern. We also built an image of the second Stokes parameter (Fig. 4a). Similar images were constructed in [2,8,9,13,14]. They are considered to characterize the distribution of the average particle size over the lunar surface. Finally, we calculate the phase ratio $S(87°)/S(63°)$ shown in Fig. 4b, where $S(\alpha)= A_\perp(\alpha)–A_\parallel(\alpha)$. This ratio image resembles the distribution shown in Fig. 3b.

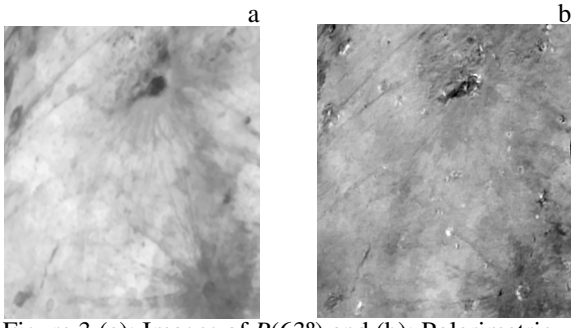

Figure 3 (a): Images of $P(63°)$ and (b): Polarimetric phase ratio $P(87°)/P(63°)$

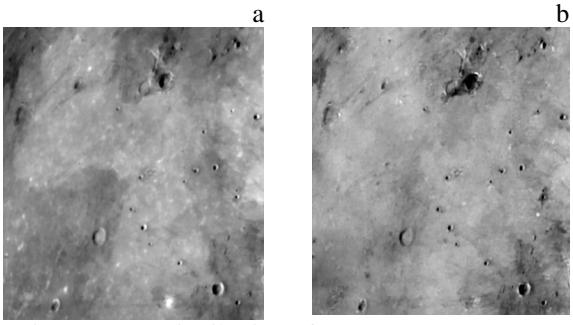

Figure 4 (a): Distribution of $S(\alpha)=A_\perp(\alpha)–A_\parallel(\alpha)$ at α=63°; (b): Phase ratio $S(87°)/S(63°)$

Conclusion: We present phase ratios of several polarimetric characteristics. Unfortunately there are currently no direct quantitative interpretations of the images shown in Fig. 1 and Fig. 2, however, they undoubtedly suggest independent information about the lunar surface and are worth further investigations using not only Earth-based observations but spacecraft measurements from a polar orbit of the Moon as well.

References: [1] Hapke B. (1993) *Theory of reflectance and emittance spectroscopy*, Cambridge Univ. Press, 450 p. [2] Shkuratov Y. (2011) *PSS 59*, 1326-1371. [3] Shkuratov Y. et al. (1994) *Icarus 109,* 168-190. [4] Kaydash V. et al. (2011) *Icarus 211,* 89–96. [5] Shkuratov Y. et al. (2013) *PSS 75,* 28–36. [6] Kaydash V. et al. (2013) *PSS 89,* 172–182. [7] Shkuratov Y. et al. (2012) *Icarus 218*, 525-533. [8] Shkuratov Y., Opanasenko N. (1992) *Icarus 99*, 468-484. [9] Shkuratov Y. et al. (2007) *Icarus 187*, 406–416. [10] Shkuratov Y. et al. (2010) *Icarus 208*, 20–30. [11] Kaydash V. et al. (2012) *JQSRT 113*, 2601-2607. [12] Jeong Minsup et al. (2016) *PASJ* doi: 10.1093/pasj/psw090. [13] Dollfus A. (1998) *Icarus 136*, 69–103. [14] Jeong Minsup et al. (2015) *Astrophys. J. Suppl. 221*, No.1.